Journal of Sound and Vibration 464 (2020) 114975

Contents lists available at ScienceDirect

Journal of Sound and Vibration

journal homepage: www.elsevier.com/locate/jsvi

On the sound field from a source moving above non-locally reacting grounds

Y. Wang [a], K.M. Li [a,*], D. Dragna [b], P. Blanc-Benon [b]

[a] Ray W. Herrick Laboratories, School of Mechanical Engineering, Purdue University, 177 S. Russell Street, West Lafayette, IN 47907-2099, USA

[b] Univ Lyon, Ecole Centrale de Lyon, INSA Lyon, Université Claude Bernard Lyon I, CNRS, Laboratoire de Mécanique des Fluides et d'Acoustique, UMR 5509, 36 Avenue Guy de Collongue, F-69134, Ecully, France

A R T I C L E I N F O

Article history:
Received 11 June 2019
Received in revised form 22 August 2019
Accepted 18 September 2019
Available online 26 September 2019
Handling editor: R.E. Musafir

Keywords:
Moving source
Asymptotic solution
Ground reflection
Doppler effect
Ground impedance
Non-locally reacting ground
Extended reaction ground

A B S T R A C T

This paper investigates the sound fields generated by a source moving horizontally at a constant speed above a non-locally reacting flat ground. The present study offers an extension of an earlier study that focused on sound fields owing to a moving source above a locally reacting ground. However, a locally reacting ground model may not be sufficient for many acoustic "soft" grounds such as snow-covered ground or a layer of sound-absorbing materials. An integral representation for the sound fields is obtained by means of a Lorentz transform. Further analysis using the steepest descent method is then applied and leads to a uniform asymptotic approximation for the total sound fields. The explicit connection between the Lorentz frame and the physical space is explored. This allows for a closed-form analytical expression written in the emission time frame for arbitrary spatial locations of a moving source and stationary receiver. The asymptotic solution is validated by comparing it with a direct numerical solution of the time-domain linearized Euler equations. The analytical solution, which is referred to as the Dopplerized Weyl-van der Pol (D-WVDP) formula, generalizes the earlier theoretical results to allow for the source motion and non-locally reacting ground surfaces. An approximation scheme can further be identified, and its range of validity is discussed.

1. Introduction

The study of noise emanating from a moving source has become more imperative in the last several decades owing to the increasing speed of modern air-based and land-based transportation vehicles. Owing to the growth of computing power, time-domain numerical approaches such as the finite-difference time-domain (FDTD) method [1,2] have gained popularity for applications in outdoor sound propagation. These approaches are particularly well-suited for use with moving sources, as they naturally account for the Doppler effect and can handle any source trajectory. Recent studies [1,3] showed interest in such approaches. It is, therefore, expedient to develop an accurate and fast computational model in order to validate the ground effect predicted by the time-domain approaches [1]. In a recent study [4], an asymptotic formula was derived for predicting the sound fields from a source moving above a locally reacting ground. However, many outdoor ground surfaces are non-locally reacting in nature. For example, snow covered grounds [5,6], forest floors [7], and railway ballast [8] are best

* Corresponding author.
E-mail addresses: wang1679@purdue.edu (Y. Wang), mmkmli@purdue.edu (K.M. Li).

https://doi.org/10.1016/j.jsv.2019.114975

modeled as non-locally reacting surfaces. Therefore, there is a need for generalizing the asymptotic formula to predict the sound fields from a source moving above a non-locally reacting ground.

Earlier research into moving source problems date back as early as the 1980s. Oie and Takeuchi [9] derived a much-simplified expression in which the ground wave term was ignored. This approximate solution can be inaccurate under near-grazing conditions. The current study aims to extend the prior studies [4,10–13] to offer a generalized expression that is simple yet accurate enough for the prediction of the sound fields above locally and non-locally reacting grounds.

It is notable that the general solution for the sound fields owing to a moving monopole in a free space is well recognized [14]. The Doppler effect is identified in the direct wave term. However, it is not properly included in the reflected wave term in which the ground's acoustical properties are calculated at a constant Dopplerized frequency [11,12]. An improved treatment of the Doppler effect on the spherical wave reflection coefficient was developed for a locally reacting ground [4,9]. Here, the development of a generalized asymptotic formula for predicting sound fields from a source traversing horizontally at a constant speed above a non-locally reacting ground is presented.

An asymptotic analysis that centers on the use of contour integration where the steepest descent path is identified is proposed for obtaining an approximation solution in the present study. Indeed, Chien and Soroka [15] derived an asymptotic formula for the sound field owing to a stationary sound source above a locally reacting ground. Their approximate solution was expressed in terms of the direct wave term and the ground-reflected wave term. Subsequent studies (e.g. Refs. [16–22]) extended the steepest descent method for different ground types and various source characteristics.

This paper has four sections. Section 2 shows a formulation of the problem. Using the standard transform for the physical space [15], the two-dimensional space-time wave equation can be adapted to yield a simpler analytical solution in the Lorentz space. By means of a convolution integral, the boundary condition can be simplified for the calculation of the ground-reflected wave. The steepest descent method is used and leads to an asymptotic solution for the boundary wave term in the Lorentz frame. It is further shown that the solution can be transformed back to the physical space, giving a closed-form solution. Section 3 discusses the ground model used in the validation process and explains how the surface wave pole can be determined. Section 4 validates the asymptotic formula by comparing the numerical results with those computed by the FDTD method. An approximation scheme for the asymptotic formula is discussed, and the condition for its validity is examined. Finally, concluding remarks are offered in Section 5.

2. Formulation of problem

2.1. Governing wave equations

In a two-dimensional rectangular coordinate system (x, z), a harmonic line source traverses horizontally in the x-direction. The airborne source has a subsonic constant speed of $c_0 M$traveling at a constant height of z_s above an extended reaction ground that is situated at the $z = 0$ line. Here, M is the source Mach number, and c_0 is the sound speed in the upper medium ($z > 0$), with the subscript 0 representing their corresponding parameters in air. Since the sound fields are different for an approaching or receding source, a careful specification of the region for the receiver is needed to facilitate the modeling process, as follows. See Fig. 1 for the geometry of the problem with the approaching source located in the $x > 0$ region.

The upper and lower media are homogeneous with the sound speeds and densities of c_j and ρ_j ($j = 0, 1$), respectively, where the subscript 1 denotes the corresponding parameters in the lower medium ($z < 0$). Since air is modeled as a non-dissipative medium independent of frequency, c_0 and ρ_0 are real parameters. It is also important to note that the extended reaction ground is modeled as a dissipative medium. Hence, c_1 and ρ_1 are complex parameters that vary with frequency. The time-domain equations governing sound propagation within the ground would therefore involve convolutions. For the sake

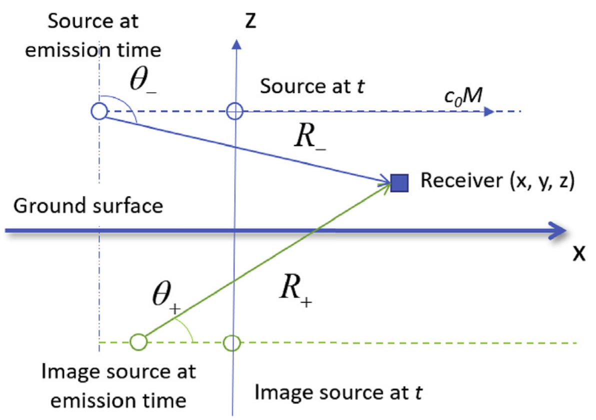

Fig. 1. Geometry of problem.

of simplicity, a frequency-domain approach is used in which the process of convolutions in the space-time domain is avoided initially.

For a sound source of unit strength, the wave equation above the ground is given in terms of the acoustic potential $\varphi_0(x,z,t)$ in the physical space-time domain by

$$\nabla^2\varphi_0 - \frac{1}{c_0^2}\frac{\partial^2\varphi_0}{\partial t^2} = \mathrm{e}^{-\mathrm{i}\omega_s t}\delta(x - c_0Mt)\delta(z - z_s), \tag{1}$$

where t is the time variable, ω_s is the angular frequency of the source in the stationary frame, the differential operator $\nabla^2 = \frac{\partial^2}{\partial x^2} + \frac{\partial^2}{\partial z^2}$, and $\delta(\cdot)$ is the Dirac delta function. Since no source is placed below the ground, the corresponding wave equation in the lower medium is simply written as

$$\nabla^2\varphi_1 - \frac{1}{c_1^2}\frac{\partial^2\varphi_1}{\partial t^2} = 0. \tag{2}$$

where $c_1 \equiv c_1(\omega)$ varies with frequency of the sound waves transmitted through the lower medium. Given the acoustic potentials $\varphi_j(x,z,t)$ (where $j = 0, 1$), the corresponding sound pressures and vertical particle velocities in the upper and lower media are determined by

$$p_j(x,z,t) = -\rho_j(\omega)\partial_t\varphi_j(x,z,t) \tag{3a}$$

and

$$v_j(x,z,t) = \partial_z\varphi_j(x,z,t), \tag{3b}$$

where $\partial_t \equiv \partial/\partial t$ and $\partial_z \equiv \partial/\partial z$. The boundary conditions for the problem are specified by requiring the continuity of pressure and normal particle velocity across the interface at $z = 0$, i.e.,

$$\rho_0\partial_t\varphi_0(x,0,t) = \rho_1\partial_t\varphi_1(x,0,t) \tag{4a}$$

and

$$\partial_z\varphi_0(x,0,t) = \partial_z\varphi_1(x,0,t). \tag{4b}$$

To solve for the sound fields in the upper medium, the Lorentz transformation can be used where the right side of Eq. (1) can be converted to a stationary line source problem by introducing a set of Lorentz variables (x_L, z_L, t_L) such that

$$\begin{cases} x_L = \gamma^2(x - c_0Mt), \\ z_L = \gamma z, \\ t_L = \gamma^2(t - Mx/c_0) \end{cases}, \tag{5a}$$

where

$$\gamma = \left(1 - M^2\right)^{-\frac{1}{2}}, \tag{5b}$$

and the subscript L symbolizes the corresponding variables in the Lorentz frame for the upper medium. Applying the Lorentz transformation, Eq. (1) can be converted to

$$\nabla_L^2\varphi_L - \frac{1}{c_0^2}\frac{\partial^2\varphi_L}{\partial t_L^2} = \gamma e^{-\mathrm{i}\omega_s(t_L + Mx_L/c_0)}\delta(x_L)\delta(z_L - z_{Ls}) \tag{6}$$

where $\varphi_L \equiv \varphi_0(x_L, z_L, t_L)$ is the acoustic potential in the Lorentz frame.

The above step is analogous to the classic method for solving a moving source problem in the absence of boundary surfaces [14]. However, the imposition of the boundary conditions poses a challenge for determining the sound field owing to the extended reaction ground. This is because the wave equation in the upper medium is now transformed into the Lorentz frame, but that in the lower medium is still kept in the original physical frame. There is a need to match these two coordinate systems at the interface in order to ensure correct application of the boundary conditions as stipulated in Eqs. (4a) and (4b).

2.2. Integral representations of acoustic potentials

To correctly impose the boundary conditions, it is convenient to express the acoustic potentials φ_0 and φ_1 in their respective integral forms. This process can be facilitated by using the space-time transformation where their Fourier transform pairs for the respective acoustic potentials are defined as

$$\widehat{\varphi}_j(k_x,z,\omega)=\int_{-\infty}^{\infty}\int_{-\infty}^{\infty}\varphi_j(x,z,t)\mathrm{e}^{-\mathrm{i}(k_x x-\omega t)}\mathrm{d}x\mathrm{d}t \tag{7a}$$

and

$$\varphi_j(x,z,t)=\frac{1}{4\pi^2}\int_{-\infty}^{\infty}\int_{-\infty}^{\infty}\widehat{\varphi}_j(k_x,z,\omega)\mathrm{e}^{\mathrm{i}(k_x x-\omega t)}\mathrm{d}k_x\mathrm{d}\omega, \tag{7b}$$

where $j=0$, 1. The variables k_x and ω, are the horizontal component of the wave vector and the varying angular frequency, respectively.

For the Lorentz space in the upper medium, the Fourier transform pair (φ_L and $\widehat{\varphi}_L$) is specified by

$$\widehat{\varphi}_L(L_x,z_L,\omega_L)=\int_{-\infty}^{\infty}\int_{-\infty}^{\infty}\varphi_L(x_L,z_L,t_L)\mathrm{e}^{-\mathrm{i}(L_x x_L-\omega_L t_L)}\mathrm{d}x_L\mathrm{d}t_L \tag{8a}$$

and

$$\varphi_L(x_L,z_L,t_L)=\frac{1}{4\pi^2}\int_{-\infty}^{\infty}\int_{-\infty}^{\infty}\widehat{\varphi}_L(L_x,z_L,\omega_L)\mathrm{e}^{\mathrm{i}(L_x x_L-\omega_L t_L)}\mathrm{d}L_x\mathrm{d}\omega_L. \tag{8b}$$

Note in Eqs. (8a) and (8b) that L_x is the horizontal component of the wave vector, and ω_L is the varying angular frequency for the Lorentz space.

Application of the Fourier transform pair in the Lorentz space leads to a simplification of Eq. (6) to give a second-order differential equation for $\widehat{\varphi}_L(L_x,z_L,\omega_L)$ in terms of z_L as

$$\frac{\partial^2\widehat{\varphi}_L}{\partial z_L^2}+L_z^2\widehat{\varphi}_L=2\pi\gamma\delta(z_L-z_{Ls})\delta(\omega_L-\omega_s), \tag{9a}$$

where L_z is the vertical component of the wave vector given by

$$L_z=+\sqrt{k_L^2-L_x^2}, \tag{9b}$$

and $k_L=\omega_s/c_0$ is the wave number in the Lorentz space. Strictly speaking, ω_L should be used instead of ω_s in defining k_L. However, the delta function $\delta(\omega_L-\omega_s)$ ensures that $\omega_L=\omega_s$ when the outer integral of Eq. (8b) is evaluated with respect to ω_L. Hence, $\omega_s$is used for defining k_L, which facilitates the subsequent presentation of the theoretical results. The solution for Eq. (9a) has the form

$$\widehat{\varphi}_L(L_x,z_L,\omega_L)=\frac{\gamma\pi}{\mathrm{i}L_z}\left[\mathrm{e}^{\mathrm{i}L_z\Delta z_-}+V\mathrm{e}^{\mathrm{i}L_z\Delta z_+}\right]\delta(\omega_L-\omega_s), \tag{10}$$

where $\Delta z_\mp$ are the respective height differences between the source and its image with the receiver, i.e., $\Delta z_\mp=|z_{Ls}\mp z_{Lr}|$, and V is the reflection factor to be determined from the boundary conditions given in Eqs. (4a) and (4b). By substituting Eq. (10) into Eq. (8b), an integral expression for the acoustic potential in the upper medium in the Lorentz space can then be obtained.

For the lower medium, the acoustic potential in the physical space is used. By substituting Eq. (9b) into Eq. (5), it is possible to obtain the following equation:

$$\frac{\partial^2\widehat{\varphi}_1}{\partial z^2}+\kappa_z^2\widehat{\varphi}_1=0, \tag{11a}$$

where κ_z is the vertical component of the wave vector given by

$$\kappa_z=+\sqrt{k_1^2-k_x^2}, \tag{11b}$$

and $k_1=\omega/c_1$ is the wave number in the physical space. For a semi-infinite lower medium ($z<0$), the transformed acoustic potential is the solution of Eq. (11a) that can be expressed as

$$\hat{\varphi}_1(k_x, z, \omega) = T\mathrm{e}^{-\mathrm{i}\kappa_z z}, \tag{12}$$

where T is the transmission factor dependent on the boundary conditions.

2.3. Boundary condition for an extended reaction ground

Using Eq. (7a), the boundary conditions given in Eq. (4) can be modified to

$$\rho_0 \hat{\varphi}_0(k_x, 0, \omega) = \rho_1(\omega)\hat{\varphi}_1(k_x, 0, \omega) \tag{13a}$$

and

$$\partial_z \hat{\varphi}_0(k_x, 0, \omega) = \partial_z \hat{\varphi}_1(k_x, 0, \omega), \tag{13b}$$

where ∂_z is the differentiation with respect to z. It follows from Eqs. (12) and (13b) that

$$\partial_z \hat{\varphi}_0(k_x, 0, \omega) = -\mathrm{i}\kappa_z \hat{\varphi}_1(k_x, 0, \omega). \tag{14}$$

Application of Eq. (14) to Eq. (13a) leads to the following boundary condition:

$$c_0 \partial_z \hat{\varphi}_0(k_x, 0, \omega) + \mathrm{i}\omega\beta\, \hat{\varphi}_0(k_x, 0, \omega) = 0, \tag{15a}$$

where $\beta[\equiv \beta(k_x, \omega)]$, which is the apparent surface admittance of the extended reaction ground, is given by

$$\beta = \zeta\sqrt{n^2 - (k_x/k_0)^2}, \tag{15b}$$

$k_0(\equiv \omega/c_0)$ is the wave number in air, ζ is the complex density ratio:

$$\zeta \equiv \zeta(\omega) = \rho_0/\rho_1(\omega), \tag{15c}$$

and n is the index of refraction:

$$n \equiv n(\omega) = c_0/c_1(\omega). \tag{15d}$$

Defining an impulse response in space-time for the apparent surface admittance:

$$\beta(k_x, \omega) = \int_{-\infty}^{\infty}\int_{-\infty}^{\infty} \hat{\beta}(x, t)\mathrm{e}^{\mathrm{i}(\omega t - k_x x)}\mathrm{d}x\mathrm{d}t, \tag{16}$$

the boundary condition [Eq. (15a)] can be converted to a twofold convolution integral in terms of the surface potential $\varphi_g(x, t) \equiv \varphi_0(x, 0, t)$:

$$c_0 \partial_z \varphi_g(x, t) - \int_{-\infty}^{\infty}\int_{-\infty}^{\infty} \hat{\beta}(x', t')\partial_t \varphi_g(x - x', t - t')\mathrm{d}t'\mathrm{d}x' = 0. \tag{17}$$

The space-time impulse response $\hat{\beta}(x, t)$ is introduced for the clarity of presentation. Its exact expression is not explicitly required in the present study. Nevertheless, more details for $\hat{\beta}(x, t)$ are discussed in Ref. [22].

The next step is to derive the corresponding boundary condition in the Lorentz space from Eq. (17). According to Eq. (5a), the differentiations with respect to t, x, and z in the physical space can be written in the Lorentz space as

$$\partial/\partial t = \gamma^2(\partial/\partial t_L - c_0 M \partial/\partial x_L) = -\mathrm{i}\omega_L \Omega, \tag{18a}$$

$$\partial/\partial x = \gamma^2[(-M/c_0)\partial/\partial t_L + \partial/\partial x_L] = \mathrm{i}k_L \Gamma, \tag{18b}$$

and

$$\partial/\partial z = \gamma\partial/\partial z_L. \tag{18c}$$

In Eqs. (18a) and (18b), the differential operators are applied to the acoustic potential $\varphi_L(x_L, z_L, t_L)$ in the Lorentz space. Given the integral representation of φ_L, *viz.* Eq. (8b), Ω and Γ can, therefore, be treated as algebraic functions in terms of ω_L and L_x as follows:

$$\Omega(L_x,\omega_L)=\gamma^2(1+ML_x\,/\,k_L) \tag{19a}$$

and

$$\Gamma(L_x,\omega_L)=\gamma^2(M+L_x\,/\,k_L). \tag{19b}$$

These two algebraic functions, Ω and Γ, are referred as the *temporal* and *spatial* Doppler terms, respectively. The reason for choosing these specific forms for the Doppler terms becomes apparent when the asymptotic solutions for the sound pressure are derived.

In the Lorentz space, the two surface potentials in Eq. (17) can be expressed as

$$\varphi_g(x,t)=\frac{1}{4\pi^2}\int\limits_{-\infty}^{\infty}\int\limits_{-\infty}^{\infty}\widehat{\varphi}_L(L_x,0,\omega_L)\mathrm{e}^{\mathrm{i}(L_xx_L-\omega_Lt_L)}\mathrm{d}L_x\mathrm{d}\omega_L \tag{20a}$$

and

$$\varphi_g(x-x',t-t')=\frac{1}{4\pi^2}\int\limits_{-\infty}^{\infty}\int\limits_{-\infty}^{\infty}\widehat{\varphi}_L(L_x,0,\omega_L)\mathrm{e}^{\mathrm{i}(L_xx_L-\omega_Lt_L)-\mathrm{i}(\Gamma k_Lx'-\Omega\omega_Lt')}\mathrm{d}L_x\mathrm{d}\omega_L. \tag{20b}$$

where Eq. (20b) is obtained by using the Lorentz transform [Eq. (5a)] with the *temporal* and *spatial* Doppler terms defined in Eqs. (19a) and (19b), respectively.

Substituting Eqs. 18–20 into Eq. (17), applying the convolution identity of Eq. (16), and manipulating the resulting expression, the boundary condition for an extended reaction ground in the Lorentz frame is then given by

$$\partial\widehat{\varphi}_L(L_x,0,\omega_L)/\partial z_L+\mathrm{i}k_L(\Omega\,/\,\gamma)\beta(\Gamma k_L,\Omega\omega_L)\widehat{\varphi}_L(L_x,0,\omega_L)=0, \tag{21a}$$

where

$$\beta(\Gamma k_L,\Omega\omega_L)=\zeta_L\sqrt{n_L^2-(\Gamma/\Omega)^2}, \tag{21b}$$

$$\zeta_L\equiv\zeta(\Omega\omega_L),\ \text{and}\ \ n_L\equiv n(\Omega\omega_L).$$

The above equation reveals that the boundary condition in the Lorentz frame has an analogous form comparable to the well-known impedance boundary condition. It is remarkable that Dragna et al. [4] used an impulse response in a onefold convolution integral for a locally reacting ground. For a source moving above an extended reaction ground, the apparent surface admittance varies both temporally and spatially; see Eqs. (19a) and (19b) for the temporal and spatial Doppler terms. Hence, Eq. (21a) offers a generalization of Dragna's result by extending their analysis to a twofold convolution integral for an extended reaction ground. Indeed, Eq. (21a) is one of the main results of the current study. To the best of our knowledge, this general form of the impedance boundary condition was not presented in any earlier studies.

2.4. Asymptotic solution for sound pressure in Lorentz frame

Substitution of Eq. (10) into (21a) with $z_L=0$ yields a solution for the reflection factor V as follows:

$$V=\frac{L_z-k_L\Omega\beta(\Gamma k_L,\Omega\omega_L)/\gamma}{L_z+k_L\Omega\beta(\Gamma k_L,\Omega\omega_L)/\gamma}. \tag{22}$$

Using Eq. (10) in Eq. (8b) with the reflection factor calculated by Eq. (22) and evaluating the outer integral with respect to ω_L, the acoustic potential can be simplified to

$$\varphi_L(x_L,z_L,t_L)=\int\limits_{-\infty}^{\infty}S_-\mathrm{d}L_x+\int\limits_{-\infty}^{\infty}S_+\mathrm{d}L_x-\int\limits_{-\infty}^{\infty}\frac{2k_s\Omega_s\beta_{L,s}S_+/\gamma}{L_z+k_s\Omega_s\beta_{L,s}/\gamma}\mathrm{d}L_x, \tag{23a}$$

where $S_\mp\,[\equiv S(\Delta\mp z)]$ is given by

$$S_\mp=S(\Delta\mp z)=\frac{\gamma\mathrm{e}^{-\mathrm{i}\omega_st_L}}{4\pi}\frac{\mathrm{e}^{\mathrm{i}[L_xx_L+L_z\Delta\mp z\,]}}{\mathrm{i}L_z}, \tag{23b}$$

and the vertical component of the wave vector is now evaluated with $k_L=\omega_L/c_0|_{\omega_L=\omega_s}=k_s$. Hence, $L_z=\sqrt{k_s^2-L_x^2}$. In Eq. (23a), the subscript s represents the evaluation of the corresponding parameters at $\omega_L=\omega_s$. For example,

$$\begin{cases} \Omega_s = \gamma^2(1 + ML_x/k_s) \\ \Gamma_s = \gamma^2(M + L_x/k_s) \\ \beta_{L,s} = \zeta_{L,s}\sqrt{n_{L,s}^2 - (\Gamma_s/\Omega_s)^2} \\ \zeta_{L,s} \equiv \zeta(\omega_s\Omega_s) \\ n_{L,s} \equiv n(\omega_s\Omega_s) \end{cases}.$$

By using the identities in Eqs. (3a), (18a) and (19a), the acoustic potential in the upper medium can be transformed from Eq. (23) to yield the sound pressure as

$$p_0(x_L, z_L, t_L) = p_- + p_+ + I_b, \tag{24a}$$

where the first two integrals can be identified as the sound fields owing to the source and its image:

$$p_\mp(x_L, z_L, t_L) = \mathrm{i}\rho_0\omega_s \int_{-\infty}^{\infty} \Omega_s S_\mp \mathrm{d}L_x, \tag{24b}$$

and the third term is the wave contribution from the boundary surface:

$$I_b(x_L, z_L, t_L) = -\frac{\gamma\rho_0\omega_s \mathrm{e}^{-\mathrm{i}\omega_s t_L}}{2\pi} \int_{-\infty}^{\infty} \frac{k_s\Omega_s^2\beta_{L,s}/\gamma}{L_z + k_s\Omega_s\beta_{L,s}/\gamma} \frac{\mathrm{e}^{\mathrm{i}[L_x x_L + L_z \Delta z_+]}}{L_z} \mathrm{d}L_x. \tag{24c}$$

Note that the first and second integrals of Eq. (24a) are identical except for the difference in the height levels at Δz_- and Δz_+, respectively. Consequently, their asymptotic solutions can be represented in a common form. Using the polar coordinate system (k_s, μ_L) to replace the wave vector (L_x, L_z), Eq. (24b) can be recast as

$$p_\mp(d_\mp, \Theta_\mp, t_L) = \mathrm{i}\rho_0\omega_s \frac{\gamma \mathrm{e}^{-\mathrm{i}\omega_s t_L}}{4\pi} \int_C \Omega_s(\mu_L) \mathrm{e}^{\mathrm{i}k_s d_\mp \cos(\mu_L - \Theta_\mp)} \mathrm{d}\mu_L, \tag{25a}$$

where $\Omega_s(\mu_L)$ can now be interpreted as the temporal Doppler factor given by

$$\Omega_s(\mu_L) = \gamma^2(1 + \overline{M}\sin\mu_L), \tag{25b}$$

$$\overline{M} = \mathrm{sgn}(x - c_0Mt)M, \tag{25c}$$

and $d_\mp = \sqrt{x_L^2 + \Delta z_\mp^2}$ are the respective radial distances centered from the source (with the negative radical in the subscript) and its image (with the positive radical) to the receiver. The modified Mach number $\overline{M}$ is used in favor of M because it can lead to a more compact expression in Eq. (25b) and in the subsequent expressions. A positive value of $\overline{M}$, $x > c_0Mt$, indicates an approaching source whereas a negative value represents a receding source.

The respective polar angles $\Theta_\mp$ in the Lorentz space are measured from the positive z_L-axis. The integration path C in Eq. (25a) starts from $-\pi/2 + \mathrm{i}\infty$ in the complex μ_L- plane, moves vertically downward to the point $-\pi/2 + 0\mathrm{i}$, horizontally to $\pi/2 + 0\mathrm{i}$, and vertically arrives at $\pi/2 - \mathrm{i}\infty$.

By means of the steepest descent method [24], the integral of Eq. (25a) can be evaluated asymptotically to offer approximate solutions for $p_\mp(d_\mp, \Theta_\mp, t_L)$ in the Lorentz space as

$$p_\mp(d_\mp, \Theta_\mp, t_L) \approx \rho_0\omega_s \frac{\gamma}{4}\Omega_\mp \mathrm{e}^{-\mathrm{i}\omega_s(t_L - d_\mp/c_0)}\sqrt{2/\mathrm{i}\pi k_s d_\mp}, \tag{26a}$$

where Ω_- and Ω_+ are the respective Doppler factors for the source and image source:

$$\Omega_\mp \equiv \Omega_s(\Theta_\mp) = \gamma^2(1 + \overline{M}\sin\Theta_\mp). \tag{26b}$$

An exact solution (expressed in terms of the Hankel function) can be identified for Eq. (25a), see Eq. (29) of [4], but it is more convenient to use Eq. (26a) in the following analysis.

Using the same polar coordinate system in the Lorentz frame, the boundary wave term can also be written analogously in an integral form as

$$I_b(d_+,\Theta_+,t_L) = -\rho_0\omega_s\frac{\gamma e^{-i\omega_s t_L}}{2\pi}\int_C \frac{(\Omega_s^2\beta_{L,s}/\gamma)e^{ik_s d_+\cos(\mu_L-\Theta_+)}}{\cos\mu_L+\Omega_s\beta_{L,s}/\gamma}d\mu_L, \tag{27a}$$

where Ω_s is given by Eq. (25b). The apparent admittance $\beta_{L,s}$ is derived from Eq. (21b) to give

$$\beta_{L,s}(\mu_L) = \zeta_{L,s}\sqrt{n_{L,s}^2-(\overline{M}+\sin\mu_L)^2/(1+\overline{M}\sin\mu_L)^2}, \tag{27b}$$

where $\zeta_{L,s}\equiv\zeta(\omega_s\Omega_s)$ and $n_{L,s}\equiv n(\omega_s\Omega_s)$.

In the Lorentz space, the reflection factor $V(\mu_L)$ [see Eq. (22)] can be transformed into the plane wave reflection coefficient:

$$V(\mu_L) = \frac{\cos\mu_L-(\Omega_s/\gamma)\zeta_{L,s}\sqrt{n_{L,s}^2-(\overline{M}+\sin\mu_L)^2/(1+\overline{M}\sin\mu_L)^2}}{\cos\mu_L+(\Omega_s/\gamma)\zeta_{L,s}\sqrt{n_{L,s}^2-(\overline{M}+\sin\mu_L)^2/(1+\overline{M}\sin\mu_L)^2}}. \tag{28}$$

The kernel function of the boundary wave term, *viz.* Eq. (27a), can then be rearranged in a recognizable form as

$$(\Omega_s/2)[1-V(\mu_L)] = \frac{(\Omega_s^2\beta_{L,s}/\gamma)}{\cos\mu_L+\Omega_s\beta_{L,s}/\gamma}. \tag{29}$$

To evaluate the integral of Eq. (27a), it is necessary to find the pole $\mu_{L,p}$, say, in the Lorentz frame. This can be done readily by setting the denominator on the right side of Eq. (29) to zero, leading to a transcendental equation in terms of $\mu_{L,p}$ as

$$\cos\mu_{L,p}+\Omega_p\beta_{L,p}/\gamma = 0, \tag{30}$$

where the subscript p represents the corresponding parameters to be evaluated at the pole location, e.g., $\Omega_p\equiv\Omega_s(\mu_{L,p})$ and $\beta_{L,p}\equiv\beta_{L,s}(\mu_{L,p})$.

With the knowledge of the pole in the integrand, Li and Tao [22] used the steepest descent method in conjunction with the pole subtraction method to evaluate this type of diffraction integral. The details of this analysis will not be repeated here, but the asymptotic solution can be summarized as follows. In the Lorentz frame, the accurate asymptotic solution for Eq. (27a) when $k_s d_+\gg 1$ can be derived to yield

$$I_b(d_+,\Theta_+,t_L) = (V_+-1)\{1-A_L F(w_{L,p})\}p_+(d_+,\Theta_+,t_L), \tag{31}$$

where $V_+ = V(\Theta)$ is the plane wave reflection coefficient (in the Lorentz frame) evaluated by Eq. (28) with $\mu_L = \Theta_+$, A_L is referred to as the augmented diffraction factor [22], and $F(\ )$ is the boundary loss factor defined by

$$F(w_{L,p}) = 1+i\sqrt{\pi}w_{L,p}e^{-w_{L,p}^2}\mathrm{erfc}(-iw_{L,p}). \tag{32a}$$

$e^{-Z^2}\mathrm{erfc}(-iZ)$ is the scaled complementary function with a complex argument Z [25], and $w_{L,p}$ is the apparent numerical distance determined by the following equation:

$$w_{L,p}^2/ik_s d_+ = 1-\cos(\mu_{L,p}-\Theta_+). \tag{32b}$$

The augmentation factor A_L is calculated by

$$A_L = \left[\frac{\Omega_p\beta_{L,p}}{\Omega_+\beta_{L,+}}\right]\left[\frac{w_{L,+}}{w_{L,p}}\right]\left[\frac{1}{\Delta_L}\right]\frac{\Omega_p}{\Omega_+}, \tag{33a}$$

where

$$\Delta_L = -\frac{d}{d\mu_{L,p}}(\cos\mu_{L,p}+\Omega_p\beta_{L,p}/\gamma), \tag{33b}$$

and $w_{L,+}$ is known as the approximate numerical distance:

$$w_{L,+} = \sqrt{\mathrm{i}k_s d_+/2}\left(\cos\Theta_+ + \Omega_+\beta_{L,+}/\gamma\right). \tag{33c}$$

Δ_L is the derivative of term $\cos\mu_L + \Omega\beta_L/\gamma$ at the pole location owing to L'Hôpital's rule. The Doppler terms and the admittance terms [see Eq. (27b) for $\beta_{L,s}$] were defined earlier, but they are presented here again for convenience:

$$\begin{cases} \Omega_p \equiv \Omega_s(\mu_{L,p}) = \gamma^2\left(1+\overline{M}\sin\mu_{L,p}\right) \\ \Omega_+ \equiv \Omega_s(\Theta_+) = \gamma^2\left(1+\overline{M}\sin\Theta_+\right) \\ \beta_{L,p} = \zeta_{L,p}\sqrt{n_{L,p}^2 - \left(\overline{M}+\sin\mu_{L,p}\right)^2\Big/\left(1+\overline{M}\sin\mu_{L,p}\right)^2} \\ \beta_{L,+} = \beta_{L,s}(\Theta_+) \end{cases}, \tag{34}$$

where the arguments for $\zeta_{L,p}$ and $n_{L,p}$ are evaluated at a frequency of $\omega_{L,p} \equiv \omega_s\Omega_p$. The frequency term $\omega_{L,p}$ and admittance term $\beta_{L,p}$ are referred to respectively as the Dopplerized pole frequency and the apparent admittance in the Lorentz frame.

Replacing the diffraction term $I_b(d_+, \Theta_+, t_L)$ in Eq. (24a) with that given by the right side of Eq. (31), the sound field in the upper medium can be determined by

$$p_0(x_L, z_L, t_L) = p_-(d_-, \Theta_-, t_L) + \left\{V_+ + A_L[1-V_+]F(w_{L,p})\right\}p_+(d_+, \Theta_+, t_L), \tag{35}$$

where $p_\mp(d_\mp, \Theta_\mp, t_L)$ are the direct and ground-reflected wave terms given by Eq. (26). All terms in Eq. (35) can be computed readily except for the factor involving Δ_L for the augmented diffraction factor A_L [see Eq. (33a)]. Using the appropriate identities of Eq. (34) in Eq. (33b), it is tedious but straightforward to derive an explicit expression for Δ_L leading to its numerical computations. For brevity, the lengthy algebraic expression for Δ_L is not presented here. Alternatively, the numerical values for Δ_L can be accurately obtained by means of the numerical differentiation of Eq. (33b). In the limiting case of a locally reacting ground, $\beta_{L,p} = \zeta_{L,p}n_{L,p}$ in Eq. (34) because $n(\omega)$ becomes large for all frequencies. Hence, a relatively simple form for Δ_L can be derived from Eq. (33b) to give

$$\Delta_L = -\sin\mu_{L,p} + \gamma\overline{M}\cos\mu_{L,p}\beta_{L,p} + \frac{\Omega_p}{\gamma}\beta'_{L,p} \tag{36}$$

where the prime in $\beta_{L,p}$ is the derivative with respect to μ_L.

Finally, all relevant functions can be assembled in Eq. (35) to arrive at the prediction of the sound fields owing to a line source moving at a constant height above a non-locally reacting ground. This is equivalent to the corresponding expression, which is Eq. (92) in Ref. [4], for the special case of a locally reacting ground.

2.5. Asymptotic formula in emission time geometry

Although Eq. (35) provides an accurate expression for computing the sound fields, it does not yield an appropriate interpretation in the physical frame for each term in the equation. It is more illuminating to present the results in a retarded time frame (i.e., the emission time geometry) instead of the Lorentz frame used in the derivation of Eq. (35). Starting from the standard two-dimensional Lorentz transformation [14], the following identities between the Lorentz space and the physical space can be established:

$$\begin{cases} x_L = \gamma^2\left(\sin\theta_\mp - \overline{M}\right)R_\mp \\ \Delta z_\mp = \gamma|z_s \mp z_r| \\ d_\mp = \gamma^2 R_\mp\Big/D_\mp \\ \cos\Theta_\mp = D_\mp\cos\theta_\mp/\gamma \\ \Omega_\mp = D_\mp \equiv D(\theta_\mp) \\ D(\theta_\mp) = 1\Big/\left(1-\overline{M}\sin\theta_\mp\right) \\ t_L - d_\mp/c_0 = t - R_\mp/c_0 \end{cases}, \tag{37}$$

where $(R_\mp, \theta_\mp)$ are the corresponding polar coordinates in the emission time geometry centered at the source and its image, and $D_\mp \equiv D(\theta_\mp)$ are the corresponding Doppler factors.

Using these identities, the sound fields owing to a moving source (p_-) and its image (p_+) can be rewritten from Eq. (26a) to give

$$p_\mp(R_\mp, \theta_\mp, t) = \frac{\rho_0\omega_s}{4}D_\mp^{3/2}\sqrt{2/\mathrm{i}\pi k_s R_\mp}\,\mathrm{e}^{-\mathrm{i}\omega_s(t-R_\mp/c_0)} \tag{38}$$

in the retarded time frame.

The kernel function of the boundary wave term, *viz.* Eq. (27a), can then be rearranged in the physical frame as

$$\frac{(\Omega_s^2\beta_{L,s}/\gamma)}{\cos\mu_L+\Omega_s\beta_{L,s}/\gamma}=\frac{\Omega_s\beta_s}{\cos\mu+\beta_s}, \tag{39a}$$

where the polar angle μ in the physical frame is introduced to replace μ_L by means of the following identities:

$$\beta_s(\mu)=\zeta_s\sqrt{n_s^2-\sin^2\mu} \tag{39b}$$

$$\cos\mu=\gamma\cos\mu_L\,/\,\Omega_s(\mu_L), \tag{39c}$$

$$\sin\mu=\frac{\overline{M}+\sin\mu_L}{1+\overline{M}\sin\mu_L}, \tag{39d}$$

and

$$D(\mu)=1\,/\,\left(1-\overline{M}\sin\mu\right)=\Omega_s(\mu_L), \tag{39e}$$

with $\zeta_s\equiv\zeta(\omega_s D)$ and $n_s\equiv n(\omega_s D)$. Eq. (39a–e) can be derived based on Eq. (37) with basic algebra.

Using Eq. (39a–e), it is possible to correlate the pole location in the Lorentz frame with that of the physical frame as follows:

$$\cos\mu_{L,p}=(D_p\,/\,\gamma)\cos\mu_p \tag{40a}$$

and

$$\sin\mu_{L,p}=D_p\left(\sin\mu_p-\overline{M}\right), \tag{40b}$$

where μ_p is the pole location in the physical frame, and $D_p\equiv D(\mu_p)$ is the Doppler term. The parameter μ_p will be referred to as the Dopplerized surface wave pole (or simply the Dopplerized pole), which indicates the effect of the source motion on the location of the pole.

To determine the Dopplerized pole, it is convenient to set the denominator on the right side of Eq. (39a) to zero. Explicit expressions for $\cos\mu_p$ and $\sin\mu_p$, which can be obtained by noting Eq. (39b), are given as follows:

$$\cos\mu_p=-\zeta_p\sqrt{\left(n_p^2-1\right)\Big/\left(1-\zeta_p^2\right)} \tag{41a}$$

and

$$\sin\mu_p=\sqrt{\left(1-\zeta_p^2n_p^2\right)\Big/\left(1-\zeta_p^2\right)}, \tag{41b}$$

where $\zeta_p\equiv\zeta(\omega_p)$, $n_p\equiv n(\omega_p)$, $\omega_p\equiv\omega_s D_p$, and the subscript p represents the parametric values evaluated at the Dopplerized pole.

The asymptotic solution for the boundary wave term can now be simplified considerably in the emission time geometry by applying the following identities for the apparent numerical distance w_p and effective numerical distance w_+:

$$w_{L,p}^2\equiv w_p^2=\mathrm{i}R_+\left(\omega_p\,/\,c_0\right)\left[1-\cos\left(\mu_p-\theta_+\right)\right] \tag{42a}$$

and

$$w_{L,+}^2\equiv w_+^2=(\mathrm{i}R_+\,/\,2)(\omega_+\,/\,c_0)[\cos\theta_++\beta_+]^2, \tag{42b}$$

where the effective admittance $\beta_+[\equiv\beta_s(\theta_+)]$ and apparent admittance $\beta_p[\equiv\beta_s(\mu_p)]$ in the emission time geometry are given respectively by

$$\beta_{L,+}=\beta_+\ \text{and} \tag{43a}$$

$$\beta_{L,p} = \beta_p, \tag{43b}$$

and $\beta_s()$ is defined in Eq. (39b).

Using the identities given in Eqs. (37), (42) a,b), and (43 a,b), the boundary wave term can be transformed from Eq. (31) into

$$I_b(R_+, \theta_+, t) = -(1 - Q)p_+(R_+, \theta_+, t), \tag{44a}$$

where Q is the spherical wave reflection coefficient:

$$Q = V_+ + A[1 - V_+]F(w_p), \tag{44b}$$

and V_+ is the plane wave reflection coefficient in the emission frame:

$$V_+ = \frac{\cos\theta_+ - \beta_+}{\cos\theta_+ + \beta_+}, \tag{44c}$$

V_+ is equal to the plane wave reflection coefficient $V(\Theta)$ in the Lorentz frame in Eq. (31).

Starting from Eq. (33a), the augmented diffraction factor A becomes

$$A = \frac{r_\beta / r_w}{\delta_\mu \Delta} \tag{45a}$$

in the physical frame where r_β is the admittance ratio:

$$r_\beta = \frac{D_p \beta_p}{D_+ \beta_+} = \frac{D_p \zeta_p \sqrt{n_p^2 - \sin^2\mu_p}}{D_+ \zeta_+ \sqrt{n_+^2 - \sin^2\theta_+}}, \tag{45b}$$

and r_w is the ratio of numerical distances:

$$r_w = \frac{w_p}{w_e} = 2\sqrt{D_p / D_+}\left[\sin\frac{1}{2}(\mu_p - \theta_+) \Big/ (\cos\theta_+ + \beta_+)\right], \tag{45c}$$

where $\zeta_+[\equiv\zeta(\omega_+)]$ and $n_+[\equiv n(\omega_+)]$ in Eq. (45a) are, respectively, the density ratio and the index of refraction calculated at the Doppler frequency $\omega_+[\equiv D_+\omega_s]$ with the Doppler factor for the image source as $D_+[\equiv 1/(1 - \overline{M}\sin\theta_+)]$. It is also possible to show that the factor Δ in Eq. (45a) can be expressed as

$$\Delta \equiv -\partial(\cos\mu_p + \beta_p) / \partial\mu_p = \sin\mu_p - \beta_p' \tag{46a}$$

where the prime in β_p represents its derivative with respect to μ_p, and $\delta_\mu$is defined as

$$\delta_\mu \equiv (D_+/\gamma)\partial\mu/\partial\mu_L|_{\mu=\mu_p} = \frac{D_+}{D_p}. \tag{46b}$$

It is important to note that Δ is different from Δ_L in Eq. (33a) and their ratio is

$$\Delta_L \Big/ \Delta = \frac{D_p}{D_+}\delta_\mu \tag{46c}$$

The rather lengthy algebraic expression for β_p' will not be presented here as it can be obtained readily with the help of the symbolic toolboxes available in MATLAB, Maple, or Mathematica.

Summing Eqs. (38) and (44a) and rearranging the resulting terms, the total sound pressure in the physical space (retarded time) can now be recast in a familiar Weyl-van der Pol (WVDP) form as

$$p_0(x_L, z_L, t_L) = p_-(R_-, \theta_-, t) + Q\ \ p_+(R_+, \theta_+, t), \tag{47}$$

where p_- and p_+ are given by Eq. (38). The above equation, which is one of the main results of the present study, generalizes WVDP for the sound field from a source moving horizontally at a constant speed above an extended reaction ground. This formula is referred to as the Dopplerized Weyl-Van der Pol (D-WVDP) formula in the following section. The first term in Eq. (47) is identified as the direct wave term, the second term is referred to as the ground reflected wave term, and Q is the spherical wave reflection coefficient.

It is worth pointing out that Eq. (47) is expressed in an asymptotic form with all terms written in the emission time geometry. In fact, the asymptotic solution for the boundary wave term, I_b, was only expressed in the Lorentz frame in most, if not all, previous studies [4,11–13]. Subsequent transformations are therefore needed to convert these numerical solutions from the Lorentz frame to the physical time frame.

3. Impedance model and dopplerized surface wave pole

Based on the D-WVDP formula [see Eq. (47)], several analyses are discussed in the following sections. Although most impedance models for a non-locally reacting ground [26] can be used in our analyses, a phenomenological model (referred to as the Hamet and Bérengier model [27]) is chosen in the present study. Three adjustable parameters, known as the airflow resistivity σ_0, tortuosity q^2, and porosity of the air-filled connected pores ϕ, are used to model a rigid porous medium in which the density ratio $\zeta(\omega)$ and the index of refraction $n(\omega)$ are calculated by

$$\zeta(\omega) = \rho_0 / \rho_1 = \phi \Big/ \left(q^2 \Gamma_\mu\right) \tag{48a}$$

and

$$n(\omega) = k_1 / k_0 = q\Gamma_\mu^{1/2}[\upsilon - (\upsilon - 1)/\Gamma_\theta]^{1/2}, \tag{48b}$$

where υ is the ratio of specific heat for air. The functions Γ_μ and Γ_θ are respectively used to model the viscous and thermal effects on the interaction of sound with the ground surface. They are determined by

$$\Gamma_\mu(\omega) = 1 + \mathrm{i}\phi\sigma_0 \Big/ \left(\omega\rho_0 q^2\right) \tag{49a}$$

and

$$\Gamma_\theta(\omega) = 1 + \mathrm{i}\sigma_0 / (\omega\rho_0 \mathrm{Pr}), \tag{49b}$$

where Pr is the Prandtl number of air. The respective numerical values of 1.22 kg m^{-3}, 1.4, and 0.72 for ρ_0, υ, and Pr are used in all computations described below.

When the Dopplerized pole μ_p is determined, both ζ and n [calculated respectively by Eqs. (48a) and (48b)] are dependent on the complex frequency ω_p instead of the constant source frequency ω_s. These ground characteristic functions ζ and n vary with the Dopplerized frequency ω_+ when the effective admittance [see Eq. (43a)] is determined. Consequently, the Doppler effect causes an apparent change in the acoustical properties of the ground surface as a result of the source motion. These subtle changes have significant impacts on the calculation of the ground reflected wave term.

The excess attenuation (EA), which is introduced to facilitate the presentation of numerical results, is defined as

$$EA = 20\,\log_{10}(p_0 / p_-) \tag{50a}$$

where p_0 is the total sound field calculated by Eq. (35), and p_- is the direct wave term given in Eq. (38). The sound pressure level (SPL), which is used in some of the plots of the current study, is defined as

$$\mathrm{SPL} = 20\,\log_{10}\left(p_0 \Big/ p_{ref}\right) \tag{50b}$$

where the reference pressure, p_{ref}, is set at 20 μPa.

Since ζ_p and n_p are functions of the Dopplerized pole, the solution to Eq. (41a) can be found straightforwardly by a simple iterative scheme for a given value of$\overline{M}$. Note here that a positive value of $\overline{M}$ gives the condition of an approaching source, while a negative $\overline{M}$ represents the condition of a receding source.

A close examination of Eq. (41a) reveals that the Dopplerized pole does not change with the source/receiver geometry but is only dependent on the acoustical property of the ground and the convection speed of the source. The Newton–Raphson method is used to find the pole location. If $\mu_p^{(j)}$ is the jth iterative solution, then the sequence $\mu_p^{(0)}$, $\mu_p^{(1)}$, $\mu_p^{(2)}$, … converges to the required pole. The recursive formula becomes

$$\mu_p^{(j+1)} = \mu_p^{(j)} - \left(\cos\mu_p^{(j)} + \beta_p^{(j)}\right) \Big/ \Delta^{(j)}, \tag{51}$$

where the superscript j indicates the corresponding function values at the jth iteration. The iteration starts with an initial guess where $\omega_p = \omega_s$ and $D_p = 1$ are used for calculating $\zeta_p^{(0)}$, $n_p^{(0)}$, and $\Delta^{(0)}$. Their use provides the first iterative solution for the Dopplerized pole in Eq. (41a). The first estimated $\mu_p^{(1)}$ is then used to calculate a revised $\zeta_p^{(1)}$, $n_p^{(1)}$, and $\Delta^{(1)}$, where the respective variables are set to $\omega_p^{(1)} = \omega_s D_p^{(1)}$ and $D_p^{(1)} = 1/(1 - \overline{M}\sin\mu_p^{(1)})$. The "new" Dopplerized pole, $\mu_p^{(2)}$, is then determined from Eq. (51). This iterative process repeats until this surface wave pole converges to the required accuracy. Typically, fewer than 10 iterations are needed to arrive at a converged solution accurate to within 10^{-16} for $|\mu_p|$.

Using the above numerical scheme, Fig. 2a demonstrates a tracing of the pole locations with $\overline{M}$ varying between 0 and $\pm$ 0.8 for an approaching and receding source. An airflow resistivity of 5 kPa m s^{-2}, tortuosity of 0.6, porosity of 0.6, and source frequency of 100 Hz are used in the plot. Fig. 2b–d shows the respective numerical results for a fixed $\overline{M} = \pm 0.5$. However, two of the three ground parameters are held constant at the same nominal values used in Fig. 2a, but the third parameter is allowed to vary over a useful parametric range. These three additional figures, which are self-explanatory, serve to highlight the effect of each ground parameter σ_0, q^2, and ϕ on μ_p.

For comparison, the respective locations of the surface wave pole for the locally reacting (LR), extended reaction (ER), and hardback (HB) ground with a layer thickness of 0.12 m are also traced in the figures. Details for modeling the HB ground are provided in the appendix for information. In addition to the pole locations, the original integration path and steepest descent path are shown in all subplots. These two paths are referred to, respectively, as OP and SDP, and are marked explicitly in Fig. 2d for information. It is well-known that surface waves are triggered if and only if the pole location is sandwiched between OP and SDP [11]. Since the SDP differs as the source traverses horizontally, only the most critical one (i.e., the grazing propagation with the saddle point located at $\pi/2$) is shown in these figures for reference.

The primary aim of the present study is to provide a generalization of the asymptotic formula for predicting the sound fields due to a monopole source moving close to an outdoor ground surface. In the numerical simulations shown in Section 4, the source speeds and the ground parameters are chosen to ensure a non-negligible presence of a surface wave component in

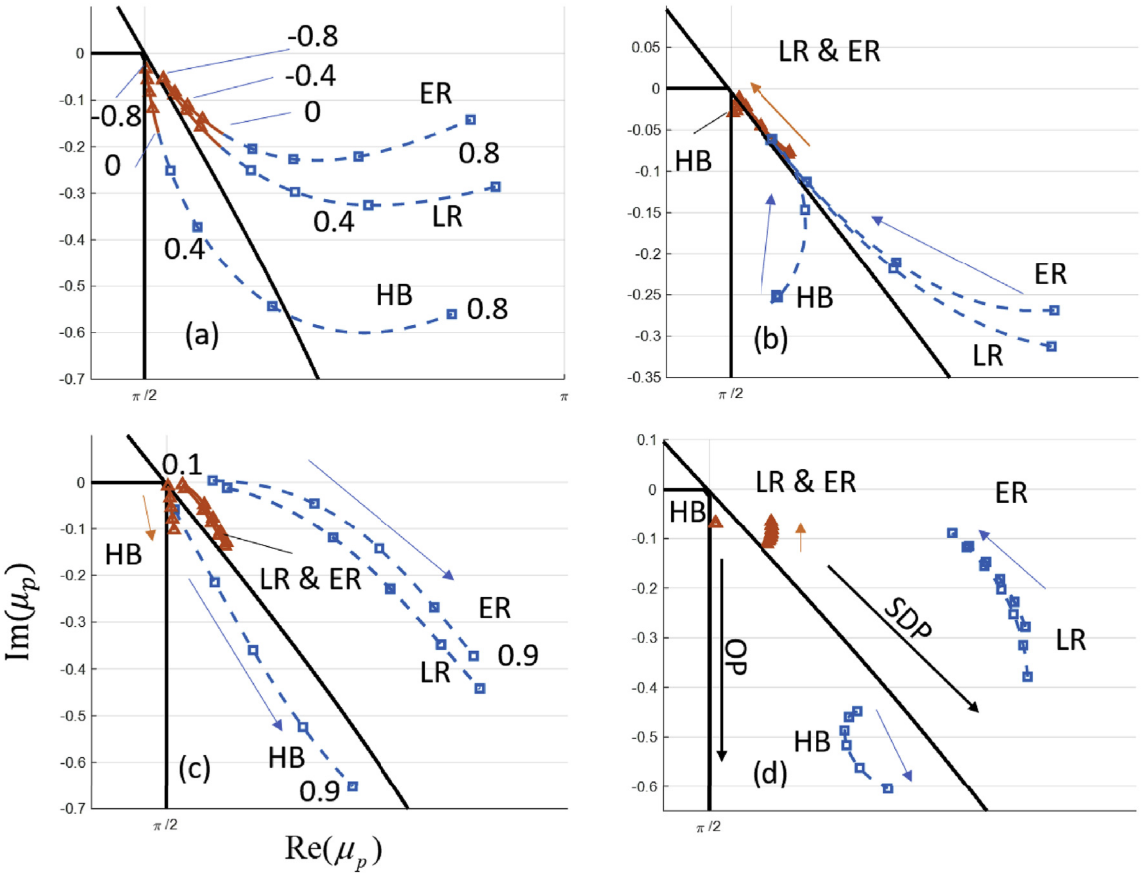

Fig. 2. Variation in pole locations with changes in Mach number and ground properties. Source frequency is set at 100 Hz and source/receiver heights at 0.3 and 0.6 m, respectively. Other symbols are as follows. SDP: steepest descent path, OP: original path of integration, LR: locally reacting ground, ER: extended reaction ground, and HB: hardback layered ground. SDP and OP are shown in all graphs and are only marked explicitly in 2(d). (a) $\overline{M}$ varies from −0.8 to 0 (solid lines with triangles) and from 0 to 0.8 (dashed lines with squares) at a step of 0.2. Ground property is kept unchanged at σ_0 . q^2 and ϕ of 5 kPa m s^{-2} are 1.2^2 and 0.6, respectively. (b) σ_0 varies from 10 to 500 kPa m s^{-2}. Other ground properties q^2 and ϕ are set at 1.2^2 and 0.6, respectively. Dashed lines with squares (approaching source): $\overline{M}$ = 0.5, and solid lines with triangles (receding source): $\overline{M}$ = −0.5. Arrows indicate direction of increasing σ_0. (c) ϕ varies from 0.1 to 0.9. Other ground properties σ_0 and q^2 are set at 5 kPa m s^{-2} and 1.2^2, respectively. dashed lines with squares (approaching source): $\overline{M}$ = 0.5, and solid lines with triangles (receding source): $\overline{M}$ = −0.5. Arrows indicate directions of increasing ϕ. (d)q^2 Varies from 1.0 to 4.0. Other ground properties σ_0 and ϕ are set at 5 kPa m s^{-2} and 0.6, respectively. dashed lines with squares (approaching source): $\overline{M}$ = 0.5, and solid lines with triangles (receding source): $\overline{M}$ = −0.5. Arrows indicate directions of increasing q^2.

the predicted sound fields. Furthermore, a realistic geometrical configuration of the source and receiver positions are selected for presenting the numerical results. These results allow thorough examinations of the relative importance of the direct wave term and various components of the ground reflected wave term. The impact on the prediction of sound fields due to the change in ground parameters, which is a subject of future studies, will not be pursued here for succinctness.

4. Validity of asymptotic formula and its approximations

4.1. Numerical validation

As described in Section 3, the Dopplerized pole can be determined numerically and can subsequently be used in Eq. (47) for calculating the sound field above a non-locally reacting ground. In order to confirm the validity of the D-WWDP formula [cf. Eq. (47)], comparisons are carried out with a direct numerical solution of Eqs. (1) and (2) using a FDTD approach. For this, an FDTD solver [4,29] is used. The computational domain in the FDTD solver is split into two subdomains. The linearized Euler equations are solved for the acoustic pressure in air for the upper domain. The lower computation domain corresponds to the ground in which time-domain equations associated with the Hamet and Bérengier model are solved. A brief derivation of these equations is given in Appendix B. As in Ref. [4], a Gaussian source is employed to model the theoretical Dirac delta function source. The width of the Gaussian B should be as small as possible in order to avoid non-compacity effects [3] and consider that the Gaussian source behaves as a point source. In all simulations, the parameter $k_sB/(1-M)$ is kept below 0.3. Hence, the validity of the D-WWDP formula [cf. Eq. (47)] can be confirmed by comparing its numerical solutions with those obtained by the FDTD methods.

Comparisons were conducted for a range of different values of M, σ_0, q^2, and ϕ. Typical time histories for the predicted sound pressure levels (SPL) are summarized for a source moving above an ER ground and an HB ground with a layer thickness of 0.15 m in Fig. 3a and b, respectively. In Fig. 3a, $M = 0.5$, $\sigma_0 = 1.0$ kPa s m^{-2}, $q^2 = 1.8^2$, and $\phi = 0.5$ are used in the numerical simulations. On the other hand, $M = 0.3$, $\sigma_0 = 10.0$ kPa s m^{-2}, $q^2 = 1.25^2$, and $\phi = 0.5$ are selected for the HB ground in Fig. 3b. A source frequency of 300 Hz is used in both plots, where the solid lines indicate the numerical results according to the FDTD method, and the circles (◯) are those obtained by the asymptotic formula. The source moves at respective heights of 2 m and 0.5 m above the ER and HB grounds. The receiver is placed at different heights of 0, 2, and 5 m above the ground in both cases. The predicted sound fields emitted by a source moving above an LR ground (using the identical ground parameters and the same source/receiver geometry) are also presented. They are shown as crosses (×) in these two figures for the purpose of illustration. It is worth noting that the ground wave term plays a more important role in predicting the total sound fields for the near-grazing propagation. Use of an LR ground model for the ER and HB grounds therefore becomes increasingly inadequate when the receiver is located in the vicinity of the ground surface.

In the predicted sound fields above the non-locally reacting ground, outstanding agreements between the D-WVDP formula and those obtained by the FDTD method are evinced in Fig. 3 and b. The levels of agreement between these two

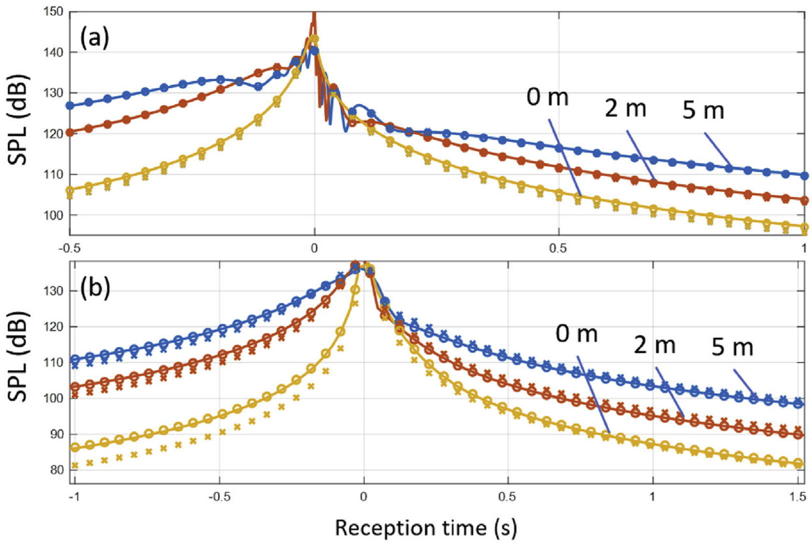

Fig. 3. Comparisons between asymptotic solutions of locally reacting model (×) and non-locally reacting model (◯) with time-domain finite difference solutions (solid lines). Reference sound pressure is 20 μPa for SPL calculation. Receiver is located at 0, 2, and 5 m above the ground. x coordinates of source and receiver are both 0 when reception time is 0. Harmonic source has frequency of 300 Hz. (a) Semi-infinite extended reaction ground: source moves at constant height of 2 m above the ground with Mach number of 0.5. Ground has σ_0 , q^2, and ϕ of 1 kPa m s^{-2}, 1.8^2, and 0.5, respectively. (b) Hardback ground with layer thickness of 0.15 m: source moves at constant height of 0.5 m above the ground with Mach number of 0.3. Ground has σ_0 , q^2, and ϕ of 10 kPa m s^{-2}, 1.25^2, and 0.5, respectively.

numerical schemes are excellent for all other source/receiver geometries and ground surfaces. These comparisons mutually validate the adequacy of either method as a tool to predict the sound fields from a source moving above a non-locally reacting ground.

4.2. Validity of different approximate schemes

In Section 3.5, the D-WVDP formula was derived for predicting sound fields owing to a source moving horizontally at a constant speed above a non-locally reacting ground. The accuracy of the D-WVDP formula was confirmed in Section 4.1, and the validity of various approximate schemes will be examined in this section. By using Eqs. (44b) and (47), the D-WVDP formula can be re-arranged as follows:

$$p_0 = [p_- + V_+ p_+] + A[1 - V_+]F(w_p)p_+, \tag{52}$$

for facilitating discussion. The first two terms in Eq. (52) are grouped together in square brackets. They are known as a sum of the contributions from the direct and specularly reflected waves. The third component, which is known as the ground wave (GW) term, is needed for accurate prediction of near-grazing situations [28].

For non-near-grazing propagation (i.e., $|\theta_+|$ is less than around 85°), the steepest descent path lies away from the surface wave pole. In this case, the pole has minimal effects on the evaluation of the integral of Eq. (27b). The Dopplerized boundary loss factor term $F(w_p)$ becomes negligibly small. This implies that the GW term has an insignificant contribution to the D-WVDP formula. If a further approximation is made such that $\overline{M}\sin\theta_+ \to 0$, then $\omega_+ \approx \omega_s$ because $D_+ \to 1$. The acoustical characteristics of the ground can therefore be evaluated at the source frequency. The D-WVDP formula can then be approximated by

$$p_0 = p_- + \frac{\cos\theta_+ - \beta_s}{\cos\theta_+ + \beta_s} p_+, \tag{53}$$

and $\beta_s = \zeta_s\sqrt{n_s^2 - \sin^2\theta_+}$ for an ER ground. This approximate solution is analogous to the expression given in Ref. [9]. It is clear in Eq. (53) that $\beta_s = \zeta_s n_s$ for an LR ground, and $\beta_s = -\mathrm{i}\zeta_s\sqrt{n_s^2 - \sin^2\theta_+}\tan(k_s d\sqrt{n_s^2 - \sin^2\theta_+})$ for an HB ground.

Equation (53) has a limited range of applicability owing to the assumption of a small $\overline{M}\sin\theta_+$. An improvement was highlighted by Ochmann [13], who argued that the Dopplerized frequency ω_+ should be used instead of the source frequency ω_s. A heuristic modification can simply be obtained by using the "Dopplerized" plane wave reflection coefficient [cf. Eq. (44c) for the emission time frame and Eq. (28) for the Lorentz frame] in Eq. (53). The resulting formula is essentially the sum of the direct and specular wave terms, i.e., the first square-bracketed term in Eq. (52).

A further improvement can be identified by using a pseudo-stationary source approach as follows. First, the source frequency is kept constant at ω_+ instead of ω_s. Second, a retarded-time algorithm [12] is used at each time step for determining the relative positions of the receiver and the moving source. The source is then "frozen" at the spatial position corresponding to each time step where ω_+ is different in each position. Finally, a saddle path integral is set up using this information for the source/receiver locations to arrive at an approximate solution as [22].

$$p_0 = p_A + [1 - V_+]F(w_+)p_+, \tag{54a}$$

where A is approximated as 1 in the GW term for a stationary source. The sum of contributions from the direct and specularly reflected waves is given by

$$p_A = p_- + \frac{\cos\theta_+ - \beta_+}{\cos\theta_+ + \beta_+} p_+. \tag{54b}$$

For a near-grazing sound propagation, Eq. (54a) is identical to the approximate solution presented by Dragna and Blanc-Benon [their Eq. (100)] [4]. They demonstrated the adequacy and necessity of using Eq. (54a) for computing the sound fields owing to a moving source placed above an LR ground. Nevertheless, it is reassuring to show that the same approximate scheme, as shown in Eq. (54a), can be modified straightforwardly to compute the sound fields above a non-locally reacting ground.

Generally speaking, Eq. (54a) gives sufficiently accurate solutions for the cases of LR and ER grounds. The difference in the computational results using Eqs. (52) and (54a) is typically less than 0.5 dB for all time steps with a traversing source and a host of different ground parameters. For brevity, these comparisons are not shown here. However, this is not precisely the case when the numerical results for an HB ground are considered.

Fig. 4 shows two sets of comparisons for an ER ground and an HB layered ground. The time histories of the excess attenuation (EA) are plotted to illustrate the accuracy of the approximate formula [Eq. (54a)] compared with the D-WVDP formula [Eq. (52)]. To have a clear presentation of these sets of results, the time scale is shown in the lower abscissa for Fig. 4a. The upper abscissa, which is shifted to the left by 0.2 s, is used for Fig. 4b. The following parameters are used in Fig. 4a. The HB ground has a layer thickness of 0.5 m, source frequency of 400 Hz, and source and receiver heights of 0.5 and of 0.2 m, respectively. The respective parameters of 0.12 m, 100 Hz, 0.6 m, and 0.3 m are used in Fig. 4b. For all plots in Fig. 4, the same

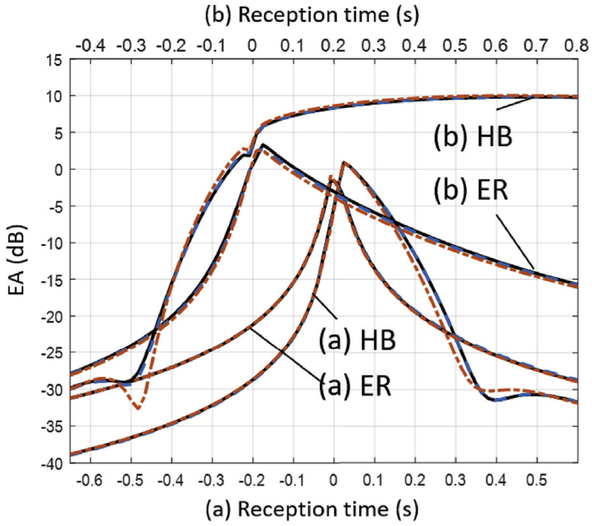

Fig. 4. Comparisons between time histories of excess attenuation (*EA*) function of asymptotic solution (dashed lines), approximated solution (dash-dotted lines) and accurate numerical integration solution (solid lines). ER: extended reaction, and HB: hardback layered ground. The *x*-coordinates of source and receiver are both 0 when reception time is 0. (a) $M = 0.3$ and source frequency is 400 Hz. The source and receiver heights are set at 0.2 and 0.5 m above the ground. The ground has σ_0 , q^2, and ϕ of 5 kPa m s^{-2}, 1.44, and 0.9, respectively. The HB ground has a layer thickness of 0.05 m. (b) Same Mach number as (a) but the source frequency is 100 Hz. The source and receiver heights are set differently at 0.3 and 0.6 m above the ground. The HB ground has a layer thickness of 0.12 m. The ground parameters are the same as (a) above. Reception time of (b) is shifted left by 0.2 s and uses top abscissa as the scale for reception time.

source speed ($M = 0.3$) and identical ground parameters ($\sigma_0 = 5.0$ kPa s m^{-2}, $q^2 = 1.25^2$, and $\phi = 0.9$) are used in the numerical simulations.

As demonstrated in Ref. [4], the error of using Eq. (54a) is negligibly small for predicting the sound fields above an LR ground. However, it can be observed from Fig. 4 and b that there are noticeable discrepancies when Eq. (54a) is used to predict the acoustic pressures above an ER ground, but the error is generally less than 0.5 dB for all time steps. The level of discrepancies becomes more acute at some time steps for an HB layered ground. The maximum discrepancy reaches an order of about 3 dB at some time steps, although the approximate solution [Eq. (54a)] agrees quite well with the general trend in the EA predicted by Eq. (52).

It is beneficial to isolate the possible bases of errors in Eq. (54a) when it is used in lieu of Eq. (52). Comparisons of Eqs. (52) and (54a) make it clear that both equations have identical p_A. The source of errors comes solely from the computation of the GW, the third term in both equations. In fact, the first error is caused by the substitution of the augmented diffraction term A with 1 in Eq. (54a). The second error is introduced in $F(w_p)$ because the effective numerical distance w_+ is used to replace the apparent numerical distance w_p in the approximation. By defining these two errors as

$$E_1 = 20\ \log_{10}|A| \tag{55a}$$

and

$$E_2 = 20\ \log_{10}\left|F(w_p)\ /\ F(w_+)\right|, \tag{55b}$$

respectively, it is instructive to plot the time histories of E_1 (dotted lines) and E_2 (dash-dotted lines) in Fig. 5. The corresponding incident angle in the physical frame, θ_+, is marked at the top abscissa for ease of reference. Three sets of graphs are displayed for (a) an HB ground with a layered thickness of 0.05 m, (b) an ER ground, and (c) an LR ground. In these graphs, the same M, z_s, z, and ground parameters are chosen for illustration (see the captions for their details). The EA predictions of p_A (dashed lines) and the GW term (solid) are presented in Fig. 6.

To have an obvious error in the approximation calculated with Eq. (54a), two conditions must be met at the same time. First, the pole must be badly predicted with the approximation, which means E_1 or E_2 must be at least 1 dB. Second, the magnitude of the GW component must be comparable to that of p_A. These two conditions can be easily met for the HB layered ground at frequencies between 100 Hz and 500 Hz. However, for the ER and LR grounds, the contribution of the surface wave component is often too small to influence the total sound fields, although the GW term and A are often poorly approximated.

Validation of the above statements can be found in Figs. 5 and 6. The GW contributions, which are considerably smaller in magnitude than p_A in the region of $|\theta_+| < 80°$, can be ignored when the sound fields are calculated. This is illustrated in their respective EA time histories shown in Fig. 6. This means that the impacts of E_1 and E_2 on the calculations of the total fields are not important, although their absolute values can exceed 3 dB in this near-overhead region. The term A can usually be approximated as 1 in the region of $|\theta_+| > 80°$ for a locally reacting ground and an extended reacting ground. However,

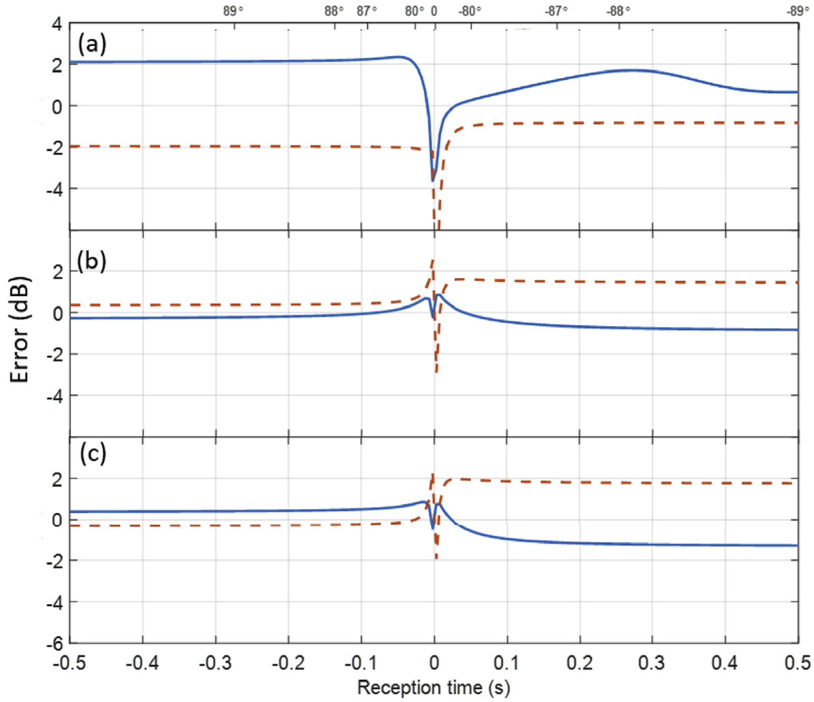

Fig. 5. Predicted time histories of E_1 (dashed lines) and E_2 (solid lines) for (a) hard-backed ground, (b) extended reaction ground, and (c) locally reacting ground. Source frequency is 400 Hz. $M = 0.3$. Source and receiver heights are set, respectively, at 0.2 and 0.5 m above the ground. The x-coordinates of the source and receiver are both 0 when reception time is 0. The layer thickness of hardback ground is 0.05 m. Ground has σ_0 , q^2, and ϕ of 5 kPa m s^{-2}, 1.44, and 0.9, respectively.

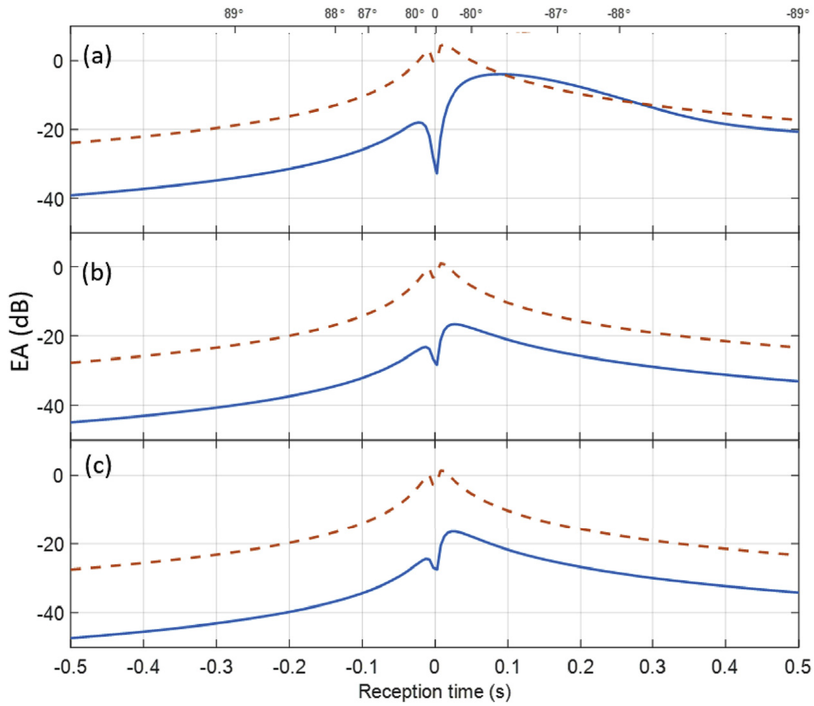

Fig. 6. Predicted time histories of p_A (dashed lines) and the ground wave term (solid lines) for (a) hard-backed ground, (b) extended reaction ground, and (c) locally reacting ground. The geometry, source speed, Mach number and ground properties are the same as those given in Fig. 5.

numerous simulations have suggested that a better agreement can be achieved if A is used instead of 1, especially for a hardback layered ground.

The error E_2 deserves more explanation as it involves calculation of the ground wave contributions. The range of variations in E_2 is greater when it is compared with that of E_1. As noted in Ref. [28], the surface wave is a separate component in the GW term, and it travels parallel and close to the porous ground. Its presence (as long as the surface wave pole is sandwiched between OP and SDP, see Fig. 2d) can impact the overall sound fields. As shown in Fig. 2a–d, the surface waves are not expected for a source moving above an LR and an ER ground if Eqs. (48a) and (48b) are used to model their acoustical characteristics. In the absence of the surface wave, the errors caused by the evaluation of GW components are limited. On the other hand, when the surface wave is present, the error E_2 can play a significant role in the prediction of the total fields; see Fig. 4a and b. As shown in Fig. 5a, a peak is observed in E_2 at $\theta_+ \approx -88^\circ$ for the HB layered ground, but there are no obvious peaks for the ER and LR grounds (see Fig. 5b and c) because there are no surface wave components in these two types of ground surfaces.

The magnitude of the GW component is another important factor that influences the total error of the approximation. An example is shown in Fig. 6 as follows. The contribution of the GW component is in excess of 10 dB higher for the HB layered ground than those for the ER and LR grounds when the reception time $t > 0$, i.e., the sound field for a receding source. As a result, E_2 causes a noticeable error in the total sound field when the approximation scheme is used. This is particularly the case when the reception time is between 0.3 s and 0.4 s; see Fig. 4a for the prediction of HB layered ground. As shown in Fig. 5b and c, E_1 and E_2 have large errors for the ER and LR grounds. However, these errors are not important since the contributions of the GW component are much smaller than p_A. Hence, the overall errors in predicting the sound fields for the ER and LR grounds are usually less than 0.5 dB.

It is also noteworthy that the errors in the total sound fields are dependent on the relative locations of the Dopplerized poles and SDP paths. There are cases when the errors in approximating the GW components are higher in the approaching region (i.e., $t < 0$) than the receding region ($t > 0$); see Fig. 4b. In general, it is found necessary to use Eq. (52) instead of Eq. (54a) in calculating the sound fields, especially for the case when the surface wave is present. Indeed, it was demonstrated by Albert et al. [31,32] for the significance of the surface wave component when they studied the propagation of sound generated by a piston shot over a thin layer of snow. Hence, it becomes evident that the use of the D-WVDP equation is particularly important for the case when the source translates above a snow-covered ground, forest floors and railway ballast.

5. Conclusion

An asymptotic formula, which is referred to as the Dopplerized Weyl-Van der Pol (D-WVDP) formula, was derived for predicting sound fields from a line source moving at a constant height above non-locally reacting grounds. Although a Lorentz frame formulation was used in the derivation, the final asymptotic solution was transformed back in the physical frame with no further approximations. The solution was written in emission time geometry where the ground effect was incorporated in the formulation. The Doppler effect not only affects the source frequency but also impacts the acoustical properties of the non-locally reacting ground.

In the current study, the Doppler effect on the ground wave term was elucidated, and the surface wave pole was examined for an approaching and receding source. The numerical solutions obtained by the D-WVDP formula were compared with the corresponding numerical solutions calculated by a heuristic approach that assumes a pseudo-stationary source. It was demonstrated that this heuristic approach yields sufficiently accurate numerical solutions for all time steps in the case of a locally reacting or an extended reaction ground. The heuristic approach can predict the general trend of the pressure time histories reasonably well in the case of a hardback layered ground. However, there are regions of disagreement in the predictions of sound fields between the D-WVDP formula and the heuristic formula. The errors in approximating the Dopplerized surface wave pole are the main “culprit” causing these disagreements (up to 3 dB) in the prediction of the total sound fields owing to a source moving at a constant speed.

Acknowledgements

The project was partially supported by Federal Aviation Administration (FAA) through ASCENT, an FAA Center of Excellence for alternative jet fuel and the environment. Opinions, findings, conclusions, and recommendations expressed in this paper are those of the authors and do not necessarily reflect the views of ASCENT sponsor organizations. The work of D. Dragna and P. Blanc-Benon was supported by the Labex CeLyA of the Université de Lyon, within the program “Investissements d'Avenir” (ANR-10-LABX-0060/ANR-16-IDEX-0005) operated by the French National Research Agency (ANR). Numerical simulations were performed using HPC resources of IDRIS under the allocation i20162a2203 made by GENCI.

Appendix A. Modification for a hardback layered ground

The admittance of a hardback layered ground is given by Ref. [21].

$$\beta_s(\mu) = -\mathrm{i}\zeta_s N_s \tan(k_s N_s d), \tag{A.1}$$

where d is the layered thickness, and

$$N_s = \sqrt{n_s^2 - \sin^2\mu}. \tag{A.2}$$

The corresponding surface wave pole, μ_p, can be determined by solving the following transcendental function:

$$\cos\mu_p - \mathrm{i}\zeta_p N_p \tan(k_s N_p d) = 0 \tag{A.3}$$

where $N_p \equiv N_s(\mu_p) = \sqrt{n_p^2 - \sin^2\mu_p}$. The second term of Eq. (A.3) can be treated as the apparent admittance of the non-locally reacting surface, $\beta_p[\equiv\beta_s(\mu_p)]$. A similar iterative scheme, which is described in Sec. 3, can be used to solve for μ_p and leads to the computation of β_p. The effective admittance of a hardback layered ground is determined explicitly by setting

$$\beta_e \equiv \beta_s(\theta_+) = -\mathrm{i}\zeta_+\sqrt{n_+^2 - \sin^2\theta_+}\tan\left(k_s\sqrt{n_+^2 - \sin^2\theta_+}\,d\right), \tag{A.4}$$

where ζ_+ and n_+ are the respective parameters evaluated at the Doppler frequency ω_+.

Appendix B. Time domain equations in rigid-frame porous media for the Hamet and Bérengier model

The time-domain Hamet and Bérengier equations, which are used in section 4, are provided in this section as follows. In the frequency domain, for an equivalent fluid (or a rigid porous medium) with density $\rho_1(\omega)$ and bulk modulus $K_1(\omega)$, the governing equations are given by

$$-\mathrm{i}\omega\boldsymbol{v}_1 + \nabla p_1/\rho_1 = 0 \tag{B1a}$$

and

$$-\mathrm{i}\omega p_1 + K_1\nabla\cdot\boldsymbol{v}_1 = 0, \tag{B1b}$$

where $\boldsymbol{v}_1 \equiv (u_1, v_1)$ is the particle velocity vector in the rigid porous medium, i.e., the extended reaction ground. Using Eq. (48) and the relation $K_1 = \rho_0 c_0^2/(\zeta n^2)$, the complex density and the bulk modulus can be written as

$$\rho_1 = \frac{\rho_0 q^2}{\phi}\left[1 + \frac{\sigma_0\phi/(\rho_0 q^2)}{-i\omega}\right] \tag{B2a}$$

and

$$K_1 = \frac{\rho_0 c_0^2}{\phi}\left[\frac{\sigma_0/(\rho_0\mathrm{Pr}) - \mathrm{i}\omega}{\nu\sigma_0/(\rho_0\mathrm{Pr}) - \mathrm{i}\omega}\right]. \tag{B2b}$$

The insertion of Eq. (B2) into Eq. (B1) yields the Hamet and Bérengier equations in the frequency domain:

$$-\mathrm{i}\omega\boldsymbol{v}_1 + \frac{\sigma_0\phi}{\rho_0 q^2}\boldsymbol{v}_1 + \frac{\phi}{\rho_0 q^2}\nabla p_1 = 0\,, \tag{B3a}$$

$$-\mathrm{i}\omega p_1 + \frac{\rho_0 c_0^2}{\phi}\left[\frac{\sigma_0/(\rho_0\mathrm{Pr}) - \mathrm{i}\omega}{\nu\sigma_0/(\rho_0\mathrm{Pr}) - \mathrm{i}\omega}\right]\nabla\cdot\boldsymbol{v}_1 = 0\,, \tag{B3b}$$

Introducing the auxiliary variable ψ defined by

$$\psi = -\frac{1}{\nu\sigma_0/(\rho_0\mathrm{Pr}) - \mathrm{i}\omega}\nabla\cdot\boldsymbol{v}_1, \tag{B4}$$

the Hamet and Bérengier equations in the time domain can then be written as a set of three first-order partial differential equations:

$$\frac{\partial\boldsymbol{v}_1}{\partial t} + \frac{\sigma_0\phi}{\rho_0 q^2}\boldsymbol{v}_1 + \frac{\phi}{\rho_0 q^2}\nabla p_1 = 0\,, \tag{B5a}$$

$$\frac{\partial p_1}{\partial t} + \frac{(\nu - 1)\sigma_0 c_0^2}{\phi \mathrm{Pr}} \psi + \frac{\rho_0 c_0^2}{\phi} \nabla \cdot \boldsymbol{v}_1 = 0 \,, \tag{B5b}$$

and

$$\frac{\partial \psi}{\partial t} + \frac{\nu \sigma_0}{\rho_0 \mathrm{Pr}} \psi + \nabla \cdot \boldsymbol{v}_1 = 0 \,. \tag{B5c}$$

The time-domain Hamet and Bérengier equations are therefore simple to solve in a FDTD approach because they do not involve convolutions. Contrary to the Wilson equations [23,30], a specific numerical method [29] is not required to solve these equations efficiently in a time-domain approach. Furthermore, the Hamet and Bérengier equations are more general than those obtained from the Zwikker and Kosten model [2]. Indeed, the present model has the correct low- and high-frequency limits (isothermal bulk modulus at low frequencies and isentropic bulk modulus at high frequencies), while the Zwikker and Kosten model assumes a constant bulk modulus. The use of Eq. (B5a)–(B5c) is therefore an interesting compromise to account for a non-locally reacting ground in the time-domain approach.

References

[1] D. Dragna, P. Blanc-Benon, Towards realistic simulations of sound radiation by moving sources in outdoor environment, Int. J. Aeroacoustics 13 (2014) 405–426.
[2] T. Van Renterghem, Efficient outdoor sound propagation modeling with the finite-difference time-domain (FDTD) method: a review, Int. J. Aeroacoustics 13 (2014) 365–404.
[3] D. Dragna, P. Blanc-Benon, F. Poisson, Modeling of broadband moving sources for time-domain simulations of outdoor sound propagation, AIAA J. (2014) 1928–1939.
[4] D. Dragna, P. Blanc-Benon, Sound radiation by a moving line source above an impedance plane with frequency-dependent properties, J. Sound Vib. 349 (2015) 259–275.
[5] O. Buser, A rigid frame model of porous media for the acoustical impedance of snow, J. Sound Vib. 111 (1986) 71–92.
[6] P. Datt, J.C. Kapil, A. Kumar, P.K. Srivastava, Experimental measurements of acoustical properties of snow and inverse characterization of its geometrical parameters, Appl. Acoust. 101 (2016) 15–23.
[7] K. Attenborough, Acoustical impedance models for outdoor ground surfaces, J. Sound Vib. 99 (1985) 521–544.
[8] K. Heutschi, Sound propagation over ballast surfaces, Acta Acustica united Acustica 95 (6) (2009) 1006–1012.
[9] S. Oie, R. Takeuchi, Sound radiation from a point source moving parallel to a plane surface of porous material, Acustica 48 (1981) 123–129.
[10] T.D. Norum, C.H. Liu, Point source moving above a finite impedance reflecting plane: experiment and theory, J. Acoust. Soc. Am. 63 (1978) 1069–1073.
[11] K. Attenborough, K.M. Li, K. Horoshenkov, Predicting Outdoor Sound, Taylor & Francis, London and New York, 2007.
[12] M. Buret, K.M. Li, K. Attenborough, Optimisation of ground attenuation for moving sound sources, Appl. Acoust. 67 (2006) 135–156.
[13] M. Ochmann, Exact solutions for sound radiation from a moving monopole above an impedance plane, J. Acoust. Soc. Am. 133 (2013) 1911–1921.
[14] P.M. Morse, K.U. Ingard, Theoretical Acoustics, Princeton University Press, 1968.
[15] C.F. Chien, W.W. Soroka, Sound propagation along an impedance plane, J. Sound Vib. 43 (1975) 9–20.
[16] K. Attenborough, S.I. Hayek, J.M. Lawther, Propagation of sound over a porous half-space, J. Acoust. Soc. Am. 65 (1980) 1493–1501.
[17] S.N. Chandler-Wilde, D.C. Hothersall, Sound propagation above an inhomogeneous impedance plane, J. Sound Vib. 98 (1985) 475–491.
[18] K.M. Li, S. Taherzadeh, K. Attenborough, Sound propagation from a dipole source near an impedance plane, J. Acoust. Soc. Am. 101 (1997) 3343–3352.
[19] K.M. Li, S. Taherzadeh, The sound field of an arbitrarily-oriented quadrupole above a ground surface, J. Acoust. Soc. Am. 102 (1997) 2050–2057.
[20] K.M. Li, S. Liu, Propagation of sound from a monopole source above an impedance-backed porous layer, J. Acoust. Soc. Am. 131 (2012) 4376–4388.
[21] K.M. Li, H. Tao, Reflection and transmission of sound from a dipole source near a rigid porous medium, Acta Acustica united Acustica 99 (2013) 703–715.
[22] K.M. Li, H. Tao, Heuristic approximations for sound fields produced by spherical waves incident on locally and non-locally reacting planar surfaces, J. Acoust. Soc. Am. 135 (2014) 58–66.
[23] D.K. Wilson, V.E. Ostashev, S.L. Collier, Time-domain equations for sound propagation in rigid-frame porous media, J. Acoust. Soc. Am. 116 (2004) 1889–1892.
[24] L.M. Brekhovskikh, Waves in Layered Media, second ed., Academic Press, New York, 1980.
[25] M. Abramowitz, I.A. Stegun, Handbook of Mathematical Functions with Formulas, Graphs and Mathematical Tables, Dover Publications, Inc., New York, 1972.
[26] K. Attenborough, I. Bashir, S. Taherzadeh, Outdoor ground impedance models, J. Acoust. Soc. Am. 129 (2011) 2806–2819.
[27] M.C. Berengier, M.R. Stinson, G.A. Daigle, J.F. Hamet, Porous road pavements: acoustical Characterization and propagation effects, J. Acoust. Soc. Am. 101 (1997) 155–162.
[28] K. Attenborough, Review of ground effects on outdoor sound propagation from continuous broadband sources, Appl. Acoust. 24 (1988) 289–319.
[29] D. Dragna, P. Pineau, P. Blanc-Benon, A generalized recursive convolution method for time-domain propagation in porous media, J. Acoust. Soc. Am. 138 (2015) 1030–1042.
[30] D.K. Wilson, V.E. Ostashev, S.L. Collier, N.P. Symons, D.F. Aldridge, D.H. Marlin, Time-domain calculations of sound interactions with outdoor ground surfaces, Appl. Acoust. 68 (2007) 173–200.
[31] D.G. Albert, Acoustic waveform inversion with application to seasonal snow covers, J. Acoust. Soc. Am. 109 (2001) 91–101.
[32] M. Boeckx, G. Jansens, W. Lauriks, D.G. Albert, Modelling acoustic surface waves above a snow layer, Acta Acustica united with Acta Acustica 90 (2004) 246–250.